Journal of Engineering Research and Reports

13(3): 8-26, 2020; Article no.JERR.56417
ISSN: 2582-2926

Numerical and Experimental Investigation on Performance of Convex-Cut Baffles in Shell-and-Tube Heat Exchanger

Moses Omolayo Petinrin[1*] and Ademola Adebukola Dare[1]

[1]Department of Mechanical Engineering, University of Ibadan, Ibadan, Nigeria.

Authors' contributions

This work was carried out in collaboration between both authors. Both authors read and approved the final manuscript.

Article Information

DOI: 10.9734/JERR/2020/v13i317101
Editor(s):
(1) Dr. Guang Yih Sheu, Chang-Jung Christian University, Taiwan.
Reviewers:
(1) Hesham Ahmed Mohamed Abdou, Egypt.
(2) M. Veera Krishna, Rayalaseeema University, India.
(3) R. S. Lebelo, Vaal University of Technology, South Africa.
Complete Peer review History: http://www.sdiarticle4.com/review-history/56417

Original Research Article

Received 24 February 2020
Accepted 30 April 2020
Published 13 June 2020

ABSTRACT

In this study, comparative performance of single-segmental baffle and a newly developed baffle – convex-cut in shell-and-tube heat exchanger were both numerically and experimentally investigated. For the numerical analysis, three working fluids (engine oil, water and air) were successively utilised on the shell-side of heat exchangers with 30, 35, 40 and 45% convex-cut (CeC_STHE) and 25% segmental (SS_STHE) baffles, and the resulting models were solved in COMSOL Multiphysics. Experiments were carried out on 30% CeC_STHE and SS_STHE exclusively running on water. The data obtained were used to determine the weighted shell-side heat transfer coefficient and weighted performance factor of each heat exchanger. Hence, the results for all the ranges of Reynolds number indicate that the shell-side heat transfer coefficients of all the CeC_STHEs are lower than that of SS_STHE except for the 30% CeC_STHE. However, the SS_STHE showed greater pressure drop than the CeC_STHEs. The choice of working fluid had more influenced on the weighted shell-side heat transfer coefficient CeC_STHE. Moreover, the weighted performance factors of the CeC_STHEs indicated positive values. Thus, 30% CeC_STHE demonstrated a better performance while the 45% had the lowest performance.

**Corresponding author: Email: mo.petinrin@ui.edu.ng, layopet01@yahoo.com;*

Keywords: Shell-and-tube heat exchangers; single-segmental baffle; convex-cut baffle; weighted performance factor; weighted heat transfer coefficient.

ABBREVIATIONS

STHE : Shell-and-Tube Heat Exchanger
A : Tube Surface Area (m^2)
c_p : Specific Heat Capacity (J/kg/K)
Δp : Pressure Drop (Pa)
ΔT_{LM} : Log Mean Temperature Difference
h : Heat Transfer Coefficient ($W/m^2/K$)
k : Thermal Conductivity of the Tube (W/m/K)
l : Characteristic Length (m)
L : Tube Length (m)
$\dot{m}$: Mass Flow Rate (kg/s)
Nu : Nusselt Number
p : Pressure (Pa)
Pr : Prandtl number
Q : Heat Transfer Rate (W)
Re : Reynolds Number
T : Temperature (K)
u : Velocity component (m/s)
x : Cartesian Coordinate (m)
WPF : Weighted Performance Factor
WSHTC : Weighted Shell-side Heat Transfer Coefficient

GREEK SYMBOLS

ρ : Density (kg/m^3)
η : Thermal Conductivity (W/m/K)
μ : Dynamic Viscosity ($Pa.s = N.s/m^2$)
ε : Dissipation Rate (m^2/s^3)

SUBSCRIPTS

av : Average
i : Inside
in : Inlet
o : Outside
out : Outlet
s : Shell
t : Tube
w : Wall

1. INTRODUCTION

Heat exchangers play vital role in process industries for proper energy utilisation and product quality in achieving system economic benefits [1]. Their wide ranges of applications are in various fields such as in power generation, refrigeration, air-conditioning, petro-chemical, petroleum refining, environment engineering, refrigeration and air-conditioning, food processing, waste energy recovery and so on [2,3]. Different varieties of heat exchangers have been developed to achieve specific purposes in industrial processes, and they are not limited to double-pipe, spiral tube, shell-and-tube, spiral, lamella, fixed matrix, brazed, plate-fin and tube-fin heat exchangers [4]. But the most widely used type is the shell-and-tube heat exchangers (STHE) which accounts for about 35 – 40% of heat exchangers found in industries [5–7]. This can be attributed to their robustness in construction, ease of maintenance, reliability and versatility for wide range of operating conditions [8,9].

The efficiency of any STHE significantly affects the overall performance of the system containing it. Thus, to improve on the economic benefit of the system, the efficiency of a STHE can only be justifiably enhanced by increasing the thermal interaction between medium separating the heat exchanger fluids and the fluids without compromising with the energy requirement of the system [10,11]. One of the best modes of enhancing the efficiency of a STHE is by inserting baffles on the shell-side. The baffles provide good support for the tubes and cause the tortuous motion of the shell-fluid for better interaction of the fluid and tube surfaces [12]. However, the overall thermo-hydraulic performance of STHEs is affected greatly by the shapes and forms of the baffles [13]. The single-segmental baffles are commonly found in STHEs for their ease of installation and striking characteristic of enhancing rate of heat transfer by turbulent mixing on the shell-side [14]. By contrast, the baffles are associated with high pressure drop, dead zones and aptness to fouling and tube vibration [15–17]. Further researches to mitigate these drawbacks have led to development of other forms of baffles such as the double-segmental, triple-segmental, no-tubes-in-window segmental, disk-and-doughnut, H-shape, helical, trefoil-hole, rod and louvre baffles [18–20].

It has been widely reported in literature that the helical baffles give better thermo-hydraulic performance than the single-segmental baffles, and that the nearness of the fluid behaviour to plug flow drastically reduces the fouling on the shell-side [6,7]. However, high manufacturing cost, difficulty in carrying out mechanical cleaning and the very high tube bundle-to-shell

flow bypass are major setbacks of the helical baffles [18,21,22].

Yongqing et al. [23] employed the experimental and numerical methods to investigate the shell-side characteristics of shell-and-tube heat exchanger with single-segmental, rod and H-shape baffles. From their results, the STHE with segmental baffles maintained higher shell-side heat transfer coefficient and pressure drop, and was followed by the STHE with H-shape baffles. Also, the H-shape baffles shared the cross-flow characteristic of the segmental baffles and longitudinal-flow characteristic of rod baffles. Yang and Liu [21] carried out both experimental and numerical studies on shell-and-tube heat exchangers with slotted baffles. In comparison of the same heat exchanger with rod baffles, they found out that the heat exchanger with slotted baffles had higher Nusselt number and pressure drop of 128–139% and 139–147%, respectively. Also, they recorded performance evaluation of 1.15–1.22 in favour of slotted baffles.

Lei et al. [8] numerically compared the performance of single-segmental and louvre baffles in shell-and-tube heat exchangers within a flow rate range. They obtained higher ratio of heat transfer coefficient to pressure drop for heat exchanger with louvre baffles as against that of segmental baffles. You et al. [22] investigated the flow and thermal characteristics of a shell-and-tube heat exchanger with trefoil baffles under turbulent flow regime, their experimental results indicated that an appreciable increase in the heat transfer rate and pressure drop as compared with STHE without baffles [24-26]. They attributed this, after a further numerical analysis, to the very high intensity and recirculation flow produced by the trefoil baffles. Other than baffle forms, there are some other details associated with baffle designs that significantly affects the thermal-hydraulic performance of shell-and-tube heat exchangers. Such as the baffle orientation and inclination, baffle cut, baffle spacing ratio, and baffle-shell clearance. Separate studies from Mellal et al. [12] and Petinrin and Dare [9] have shown that flow and thermal characteristics of STHEs are considerably altered by the baffle orientation. Also, Mohammadi et al. [27] considered horizontal and vertical baffles in the numerical analysis of shell-and-tube heat exchanger with leakage flows; findings from the study showed that the overall performance of heat exchanger with vertical baffles is higher. Leoni et al. [28] numerically assessed the effect of baffle-shell clearance on shell-side characteristics of a shell-and-tube heat exchanger, the results indicated lower pressure drop and lower shell-side outlet temperature when clearance was considered. Rahim and Jameel [29], and Raj and Ganne [30] separately carried out numerical analyses of STHEs with 0°, 10° and 20° baffle inclination angles. STHEs with 20° inclination angle were reported to have better overall performance. Ozden and Tari [31] varied baffle spacing with baffle cut (25 and 36%) in a numerical analysis of a STHE. The results obtained showed that the 25% baffle cut had better performance while the heat transfer characteristics of the heat exchanger was improved as the baffle spacing reduced.

Various configurations of baffles have been extensively used in heat exchangers to improve their performance, but none of these configurations largely due to their poor thermal ratings have shown outstanding or significant overall performance over the single-segmental baffle. Thus, this study evaluates the performance of a new baffle configuration having convex cuts through the chord of segmental baffle. Detailed numerical analysis of different geometries of this baffle in STHE will be carried out using the k-ε turbulent model. Further analysis on one of the baffle geometries will be considered using both k-ε and k-ω turbulent models and comparatively validated by carrying detailed experimental study.

2. HEAT EXCHANGER DESIGN

2.1 Geometrical Details

The convex-cut profile was formed by altering height, h or radius R, while keeping the other fixed to ensure the same area of baffle window as the single-segmental baffle (see Fig. 1). The profile radius was obtained iteratively such that the height, h was maintained at higher level than segment height, H. Thus in this study, the naming configuration of the new baffle geometries were determined from the percentage ratio of h to the baffle diameter. The nomenclature of the heat exchanger with convex-cut baffles used in this work is CeC_STHE and that of single-segmental baffles is SS_STHE. The geometrical parameters and other heat exchanger specifications are as provided in Table 1, while the thermophysical properties of the fluids are dependent on temperature.

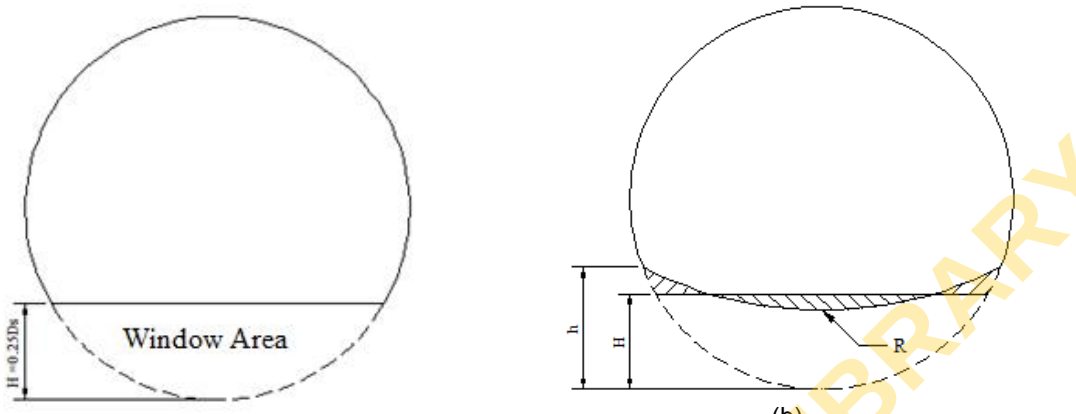

(a) (b)

Fig. 1. The profiles of the baffles (a) single-segmental and (b) convex-cut

Table 1. The geometric parameters of the heat exchangers

Component	Description	Value
Baffle	Number of Baffles, n_B	6
	Baffle Spacing, S_B	43.26 mm
	Type	Single-Segmental (H = 25%) Convex-cut (h = 30, 35, 40, 45%)
	Thickness	0.8 mm
Tube-Side	Tube Diameter, d_o	Ø15.88 mm
	Tube Length, L	302.58 mm
	Layout Pattern	Triangular (30°)
	Pitch	$1.25d_o$
	Number of Tubes, N_t	19
	Material	Copper
	Fluid	water
Shell-side	Shell Inside Diameter, D_s	Ø108.06 mm
	Inlet and Outlet Diameter (Numerical)	Ø30.00 mm
	Inlet and Outlet Diameter (Experimental)	Ø22.45 mm
	Fluid (Numerical)	engine oil, water and air
	Fluid (Experimental)	water

2.2 Numerical Analysis

2.2.1 Governing equations

The governing equations used for modelling computational domain for the fluid flow and heat transfer within the STHEs are the conservation equations for mass, momentum and energy equations as obtained from [32,33] are as stated in the following:

Continuity Equation:

$$\frac{\partial\left(\overline{\rho}\tilde{u}_j\right)}{\partial x_j}=0 \tag{1}$$

Momentum equation:

$$\frac{\partial\left(\overline{\rho}\tilde{u}_j\tilde{u}_i\right)}{\partial x_j}=-\frac{\partial\overline{p}}{\partial x_i}+\frac{\partial}{\partial x_j}\left[\left(\mu+\mu_T\right)\left(\left(\frac{\partial\tilde{u}_i}{\partial x_j}+\frac{\partial\tilde{u}_j}{\partial x_i}\right)-\frac{2}{3}\delta_{ij}\frac{\partial\tilde{u}_k}{\partial x_k}\right)-\frac{2}{3}\overline{\rho}k\delta_{ij}\right] \tag{2}$$

Energy equation:

$$\frac{\partial}{\partial x_j}\left(\bar{\rho}c_p\tilde{T}\tilde{u}_j\right)=\frac{\partial}{\partial x_j}\left(\left(\eta+\eta_T\right)\frac{\partial\tilde{T}}{\partial x_j}\right) \quad (3)$$

The *k-ε* turbulent model [33,34] was used to find the close form solution to the momentum equation and is expressed in terms of turbulent kinetic energy, *k* and the rate of dissipation, *ε* equations as

Turbulent kinetic energy:

$$\frac{\partial\left(\bar{\rho}k\tilde{u}_j\right)}{\partial x_j}=\frac{\partial}{\partial x_j}\left[\left(\mu+\frac{\mu_T}{\sigma_k}\right)\frac{\partial k}{\partial x_j}\right]+P_k-\bar{\rho}\varepsilon \quad (4)$$

Turbulent dissipation energy:

$$\frac{\partial\left(\bar{\rho}\varepsilon\tilde{u}_j\right)}{\partial x_j}=\frac{\partial}{\partial x_j}\left[\left(\mu+\frac{\mu_T}{\sigma_\varepsilon}\right)\frac{\partial\varepsilon}{\partial x_j}\right]+C_{\varepsilon1}\frac{\varepsilon}{k}P_k-C_{\varepsilon2}\rho\frac{\varepsilon^2}{k} \quad (5)$$

while the production term, P_k from equations (4) and (5) is

$$P_k=\frac{\partial\tilde{u}_i}{\partial x_j}\left[\mu_T\left(\left(\frac{\partial\tilde{u}_i}{\partial x_j}+\frac{\partial\tilde{u}_j}{\partial x_i}\right)-\frac{2}{3}\delta_{ij}\frac{\partial\tilde{u}_k}{\partial x_k}\right)-\frac{2}{3}\bar{\rho}k\delta_{ij}\right] \quad (6)$$

The *k-ε* model closure constants are $C_{\varepsilon1}$ = 1.44, $C_{\varepsilon2}$ = 1.92, C_μ = 0.09, σ_k = 1.0 and σ_ε = 1.3.

2.2.2 Boundary conditions, mesh selection and solver settings

The velocity and pressure of working fluids were initialised as zero and zero-gauge pressure, respectively. Also, the initial temperature of the computational domain was set at 303.15K. Velocity-inlet conditions were specified at the tubes- and shell-inlets with mass flow rates of 0.3 kg/s at the tube-side and 0.10 to 3.10 kg/s for engine oil and water, and 0.0025 to 0.0325 kg/s for air on shell-side. The pressure-outlet condition of 1 atm was set at the two outlets of the heat exchanger. Standard wall function was defined on the surfaces of the tubes, shell and baffles. The temperatures at the heat exchanger tube- and shell-inlets were fixed at 303.15 K and 373.15 K, respectively. Adiabatic condition was enforced on the outer surface of the shell to ensure insulated wall (Fig. 2).

The 3D computational domain was discretised into unstructured tetrahedral elements and solved by employing the finite element based CFD code, COMSOL Multiphysics. The streamline-upwind Petrov-Galerkin and Galerkin Least-Square were employed to improve on the stability and accuracy of the solution. The primitive variables were solved using three segregated solvers: Two GMRES solvers with the support of preconditioner (Incomplete LU) for velocity and pressure, and temperature; and MUMPS solver for rate of dissipation and turbulent kinetic energy.

2.3 Experimental Analysis

Both 30% CeC_STHE and SS_STHE were fabricated to make comparative performance study of the baffles. The two heat exchangers for the experimental study are as shown in Fig. 3.

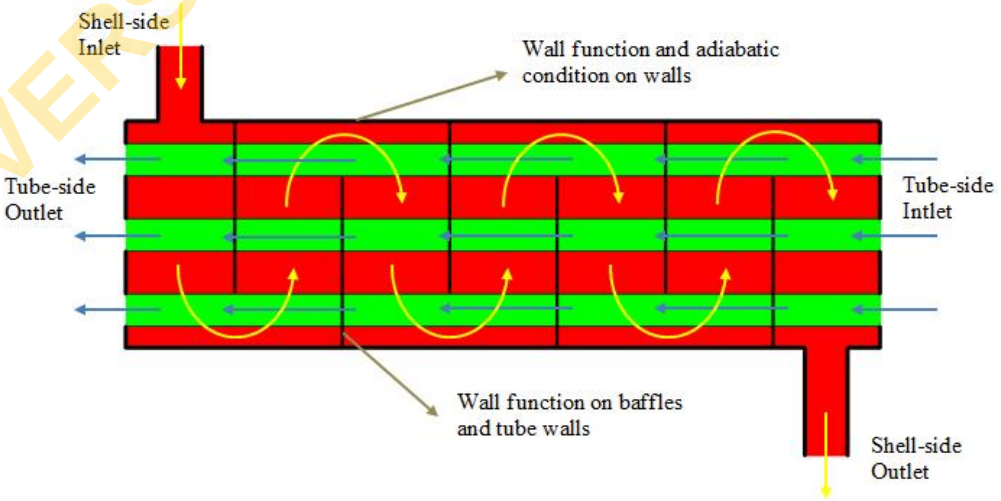

Fig. 2. The boundary conditions as prescribed for the STHEs

Fig. 3. The fabricated shell-and-tube heat exchangers

2.3.1 Experimental setup

The experimental test rig consists of each one of the heat exchangers, an electric water heater of 1.5 kW, a 200 litre water reservoir, a 372.85 W (0.5 hp) centrifugal pump, valves, two flow-meters, two pressure gauges, a thermometer, and the connecting PVC pipes, elbows and unions (Fig. 4). Five gate valves and two non-return valves (NRV) were used to regulate the flow rates of both cold and hot water streams. Digital flow-meters, namely water flow-meter and handheld ultrasonic flow-meter were used to measure the inlet flow rates, and hence compute the inlet velocities of the shell-side and tube-side of the STHE. Four type K thermocouples were installed at the inlets and outlets on both sides of the STHE and connected to read out device to measure the temperatures at these points. Two pressure gauges were also mounted at the inlet and outlet of the shell-side to measure the pressure drop within the shell-side. All these measuring devices were installed based on the instructions given in the respective operation manuals.

2.3.2 Experimental procedures and data collection

Prior to taking any data from the experimental rig, adequate measure was taken to ensure that the pipe networks were of free leakages. As shown in the Fig. 4, hot side was supplied with cold water from the water reservoir and allowed to flow until all the trapped air has been got rid of. The water heater was operated to heat up the cold water for about 50 minutes, during which the pump was also operated at intervals of 10 minutes initially and 5 minutes towards the end of the 50 minutes to recirculate and ensure a steady temperature of the heating fluid and the tube bundle. At steady state shell-side inlet temperature, the pump was left running and the cold fluid supply from the water reservoir was released and kept at a constant mass flow rate through valve, V-5. Readings were taken from all the measuring devices at varying hot water flow rates using valve, V-3 on the bypass line while keeping valve, V-4 fully opened. The average of five repeated runs at the same flow rates was calculated.

2.4 Data Reduction

2.4.1 The shell-side heat transfer coefficient

The heat exchange rate is calculated as

$$Q = \dot{m} c_p \left(T_{in} - T_{out} \right) \tag{7}$$

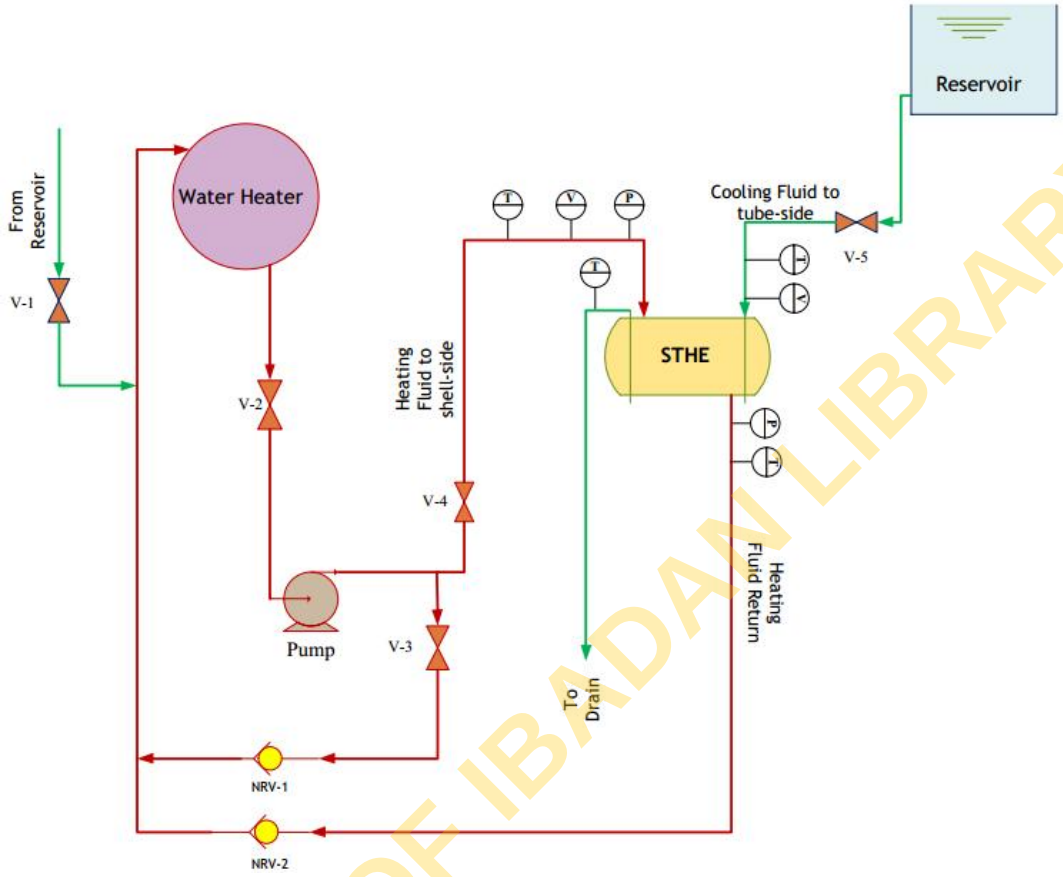

Fig. 4. The schematic representation of the experimental rig

The overall heat transfer coefficient was determined as

$$U = \frac{Q}{A_{av}\Delta T_{LM}} \tag{8}$$

With

$$\Delta T_{LM} = \frac{\left(T_{s,in} - T_{t,out}\right) - \left(T_{s,out} - T_{t,in}\right)}{\ln\left[\frac{T_{s,in} - T_{t,out}}{T_{s,out} - T_{t,in}}\right]} \tag{9}$$

The shell-side heat transfer coefficient evaluated as

$$h_o = \frac{1}{\left[A_o\left(\frac{1}{U_{av}A_{av}} - \frac{1}{h_i A_i} - \frac{\ln\left(d_o/d_i\right)}{2\pi kL}\right)\right]} \tag{10}$$

The tube-side heat transfer coefficient was determined from

$$h_i = \frac{Nu_i k}{d_i} \tag{11}$$

The tube-side Nusselt number was calculated using the Gnielinski equation [35,36] as

$$Nu_i = \frac{(\xi/8)\,\mathrm{Re}_i\,\mathrm{Pr}_i}{1+12.7\sqrt{\xi/8}\left(\mathrm{Pr}_i^{2/3}-1\right)}\left[1+\left(\frac{d_i}{L}\right)^{2/3}\right]\left(\frac{\mathrm{Pr}_i}{\mathrm{Pr}_{i,w}}\right)^{0.11} \tag{12}$$

where the friction factor, ξ is estimated from

$$\xi = \left(1.8\log(\mathrm{Re}) - 1.5\right)^{-2} \tag{13}$$

Thus, the shell-side Nusselt number can be determined as [37]

$$Nu_o = \frac{h_o l}{\eta} \tag{14}$$

where the characteristic length, l of the tube is estimated from

$$l = \frac{\pi}{2} d_o \tag{15}$$

2.4.2 The shell-side Pressure drop

For the experimental analysis, the shell-side pressure drop, Δp as obtained from [38] was determined from

$$\Delta p = p_{in} - p_{out} + \Delta p_s \tag{16}$$

where Δp_s is the hydrostatic head of water between the pressure gauges.

2.4.3 Thermo-hydraulic performance analysis of the heat exchangers

Two methods were introduced to compare the performance of heat exchanger with convex-cut baffle against that of the single segmented baffle. The first method involves the determination of equivalent shell-side heat transfer coefficient for the same pressure drop [39,40]. Therefore, the weighted average of this index over a range of Reynolds number, that is the weighted shell-side heat transfer coefficient (*WSHTC*), was determined from

$$WSHTC = \frac{1}{N} \sum_{N=1}^{N} \frac{h_{CeC} - h_{SS}}{\left(h_{CeC} + h_{SS}\right)/2} \tag{17}$$

where h_{SS} and h_{CeC} are the heat transfer coefficients of SS_STHE and CeC_STHE, respectively

The other approach uses shell-side gain factor which is the ratio of the heat duty, Q_{av} of the heat exchanger to the pumping power [27] and it is expressed as

$$\Gamma = \frac{Q_{av}}{P} \propto \frac{h}{\Delta p} \tag{18}$$

Thus, in order to determine the overall performance based on this factor, the weighted performance factor (*WPF*) for CeC_STHE at the same varying range of Reynolds numbers against the SS_STHE was obtained from

$$WPF = \frac{1}{N} \sum_{N=1}^{N} \frac{\Phi_{CeC} - \Phi_{SS}}{\left(\Phi_{CeC} + \Phi_{SS}\right)/2} \tag{19}$$

Where

$$\Phi_{CeC} = \frac{\Gamma_{CeC}}{\Gamma_{SS}} = \frac{\left(h/\Delta p\right)_{CeC}}{\left(h/\Delta p\right)_{SS}} \tag{20}$$

When either of WSHTC or WPF is greater than zero, the CeC_STHE would indicate better performance than SS_STHE but when it is less than zero, the CeC_STHE has lower performance while WSHTC or WPF of zero means equal performance of the two heat exchangers.

2.5 Uncertainty Analysis

The uncertainties of the experimental data are estimated as presented in [41,42]. Thus, the uncertainty of a desire variable, $R = f(x_i)$ can be determined from

$$\delta R = \left[\sum_{i=1}^{n} \left(\frac{\partial R}{\partial x_i} \delta x_i \right)^2 \right]^{1/2} \tag{21}$$

This is as a result of contributions of uncertainties, δx_i from a number of independent variables, x_i (i = 1, 2, . . ., n). The uncertainty of a single measured value can be obtained from

$$\delta x_i = \sqrt{B_i^2 + P_i^2} \tag{22}$$

where B is the bias error and P is the precision error of measurement.

The uncertainties obtained for the shell-side heat transfer coefficient, Nusselt number and pressure drop were ranged from 4.13 - 9.26%, 4.29 - 9.32% and 0.27 - 3.15%, respectively.

3. RESULTS AND DISCUSSION

3.1 The Shell-Side Flow and Thermal Interactions

The streamline and pressure distribution on the shell-side of the heat exchangers are as presented in Fig. 5. It is obvious that the baffle shapes affect the meandering of the fluid from the inlet-duct to the outlet-duct. The flow path of the CeC_STHE tends towards the either side of baffle-cut which reduces the fluid interaction with the tube surfaces at the baffle window but creates more cross-flow interaction. Since the exposed fraction of the tube counts is reduced at

the baffle window, the flow-induced vibration of the tubes would be reduced as could be achieved with no-tubes-in-window segmental baffles. Also, it can be seen that the pressure drop is more pronounced within the shell zones as the fluid rambles over the tube in cross-flow than the baffle windows. This is can be ascribed to the shear and pressure drags the fluid would experience in cross-flow as against the shear drag in the baffle window [43].

The temperature distributions on the shell-side of the heat exchangers are as shown in Fig. 6. It can be seen that fluid temperature reduced from the shell-inlet to its outlet due to heat rejection to the tube side. For the two heat exchangers, greater reduction in temperature can be observed in transverse flow across the tube bundles than in the longitudinal flow in the baffle windows.

The shell-side heat transfer coefficients of SS_STHE and CeC_STHE under varying Reynolds numbers for all the working fluids are as indicated in Fig. 7. From these figures, it is obvious that the heat transfer coefficient increases with the Reynolds number for each shell-side working fluid. However, for the range of Reynolds number considered for each case of water and engine oil, increase in heat transfer coefficient reduces as the Reynolds number increases; but for air, the relationship is almost linear. This trend can be ascribed to physical nature of each fluid. From Table 2, the differences in percentage of heat transfer coefficients of the SS_STHE and CeC_STHEs over the range of Reynolds number are mostly negatives, which indicate that SS_STHE demonstrated higher heat transfer coefficient except for the 30% CeC_STHE running on engine oil and water. The observed trend implies that as cut-out point of CeC_STHE increases from 30 to 45%, more of the fluid through the baffle window resorted into bypass flow, thereby reducing the fluid and tube surface interaction in cross-flow.

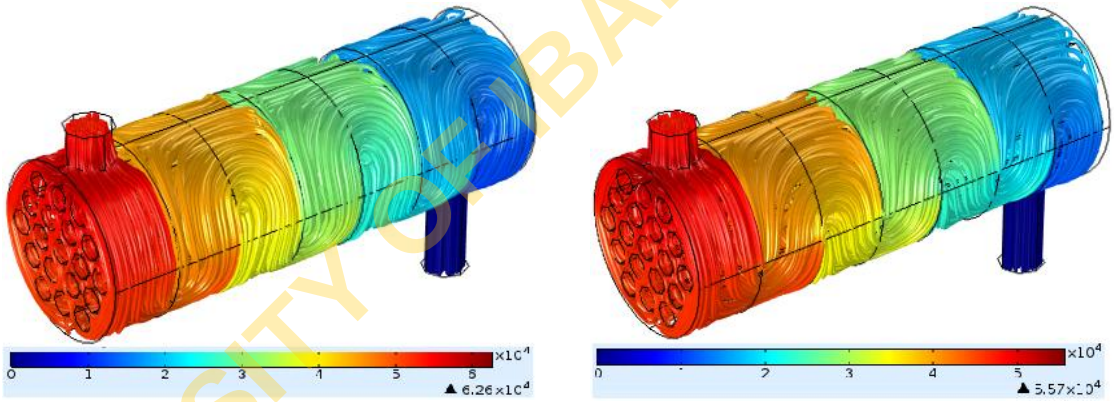

(a) (b)

Fig. 5. Velocity path lines and pressure distribution (a) SS_STHE (b) 35% CeC_STHE

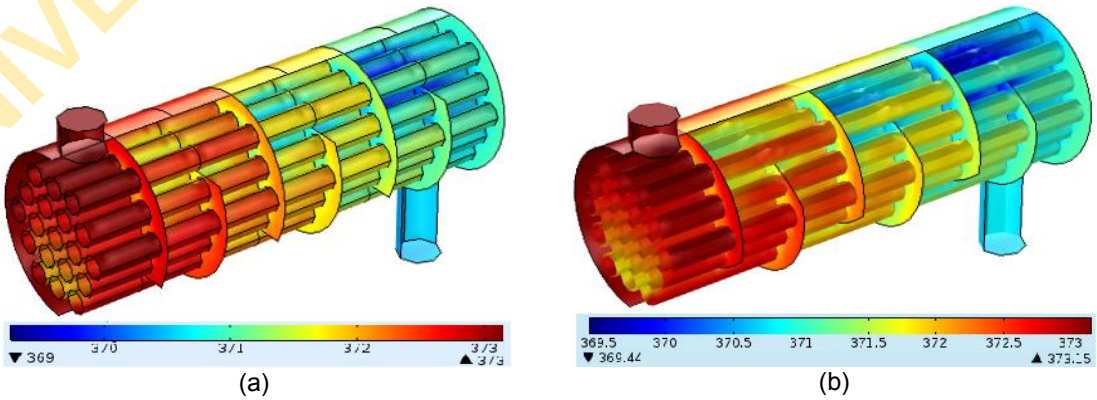

(a) (b)

Fig. 6. Temperature distribution (a) SS_STHE (b) 35% CeC_STHE

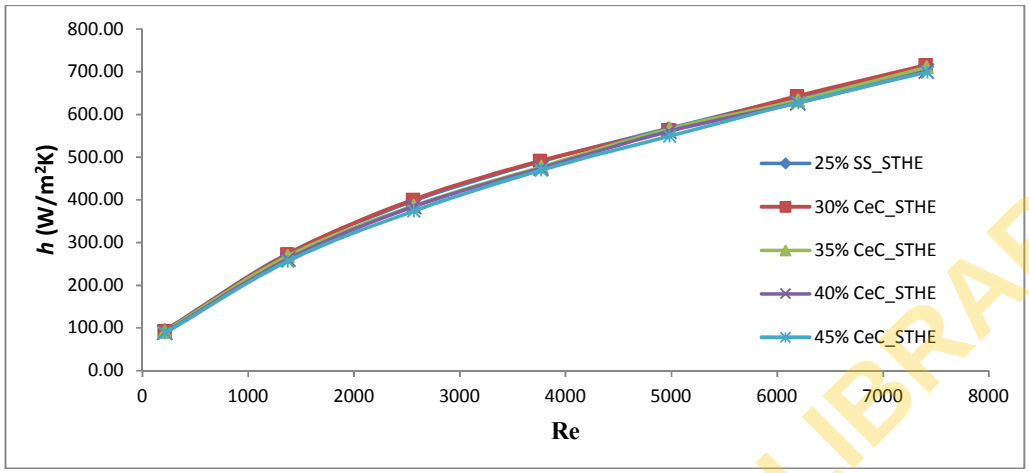

(a) Shell fluid: Engine oil

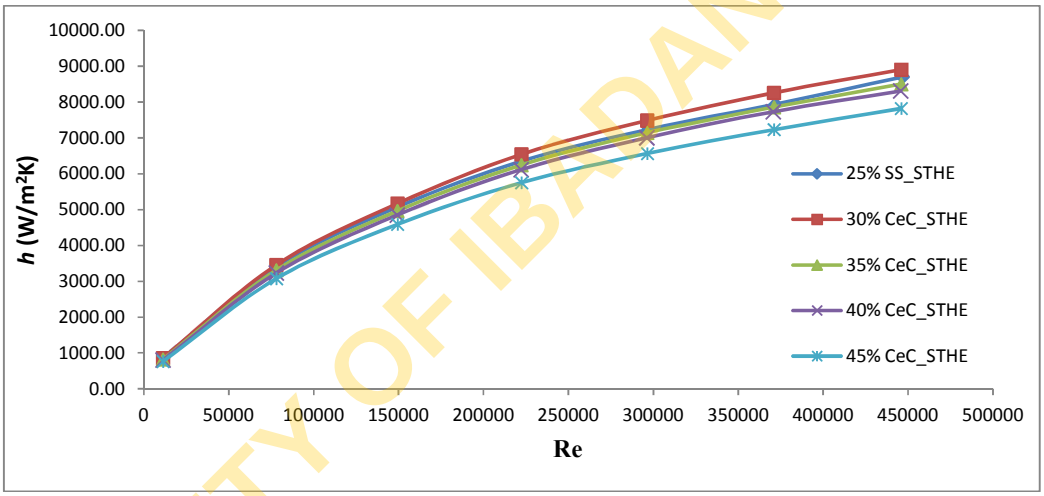

(b) Shell fluid: Water

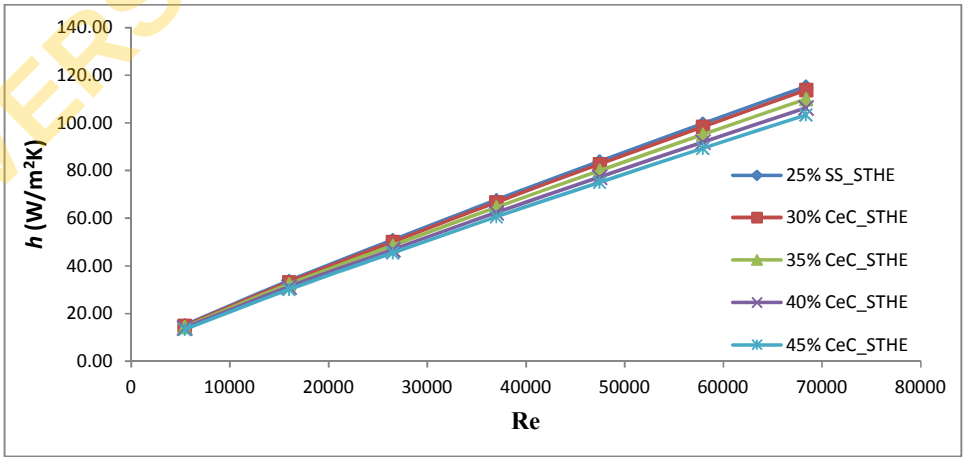

(c) Shell fluid: Air

Fig. 7. The shell-side heat transfer coefficient with Reynolds numbers

Table 2. The performance of CeC_STHEs as against SS_STHE

STHE	*h* Difference, %			Δ*p* Difference, %			WSHTC			WPF		
Model	Engine oil	Water	Air	Engine oil	Water	Air	Engine oil	Water	Air	Engine oil	Water	Air
30%	0.06	2.07	-1.48	2.17	1.22	2.24	0.007	0.023	-0.007	0.022	0.033	0.008
35%	-1.50	-2.40	-4.59	6.29	5.78	6.46	0.004	-0.013	-0.024	0.048	0.033	0.019
40%	-2.87	-4.57	-8.10	9.70	8.40	9.06	0.002	-0.029	-0.049	0.068	0.038	0.010
45%	-4.21	-10.36	-11.24	12.31	10.16	11.27	-0.002	-0.083	-0.072	0.081	-0.002	0.000

The variations of the pressure drop on the shell-side of in SS_STHE and CeC_STHE with Reynolds numbers for the working fluids are as indicated in Fig. 8. The plots in the figure show a rapid rise in pressure drop as the Reynolds number increases. This trend was also remarked by Mukherjee [44] and Zhang et al. [45], that the pressure drop increases more rapidly with increase in Reynolds number. For all the cases of the working fluids and for the same Reynolds number, the SS_STHE had higher pressure drops than CeC_STHEs as this can be seen with positive values of the percentage differences in pressure drops from Table 2.

The variation of the shell-side heat transfer coefficient and pressure drop for the working fluids in heat exchangers are as illustrated in Fig. 9. Obviously, from each figure, there is rapid increase in the pressure drop than the heat transfer coefficient as the mass flow rate keeps increasing. Similar trends were reported by Wang et al. [7,39]. The weighted shell-side heat transfer coefficients (*WSHTC*) of the heat exchangers at the same pressure drop as the SS_STHE are also presented in Table 2. Based on this performance criterion, the heat exchangers with positive weighted shell-side heat transfer coefficients are better than the SS_STHE while those ones with negative values depict poorer performance.

The performance factors of the CeC_STHEs as compared to the SS_STHE at varying Reynolds number are as indicated in Fig. 10 for engine oil, water and air respectively. From the figure, the CeC_STHEs perform better than the SS_STHE at any range of Reynolds numbers. The weighted performance factors of the CeC_STHEs for the same range of Reynolds number for each shell-side fluid are indicated in Table 2. The positive values of the weighted performance factors are indications that the heat exchangers are more desirable than the SS_STHE using this criterion.

3.2 Experimental Results

The results of the experimental study are presented in this section to show the comparative performance between the 30% CeC_STHE and SS_STHE with water as the shell-side fluid.

Fig. 11 shows the plots of shell-side heat transfer coefficient against the Reynolds number from the experimental results and in comparison with those of *k-ε* and *k-ω* turbulent models. It can be observed that the choice of numerical model affects the solution of the computational analysis but relatively from both experimental and numerical analyses, the heat transfer coefficient of the 30% CeC_STHE is higher than the SS_STHE over the Reynolds number range. The relational difference between the CeC_STHE and SS_STHE are 2.68, 5.78 and 0.94% for the experimental, *k-ε* and *k-ω*, respectively.

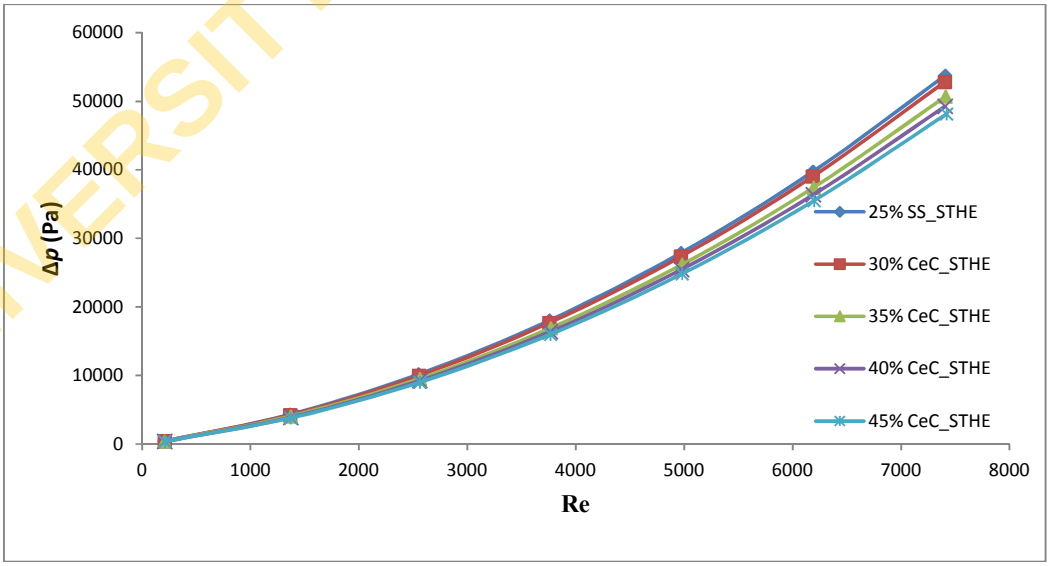

(a) Shell fluid: Engine oil

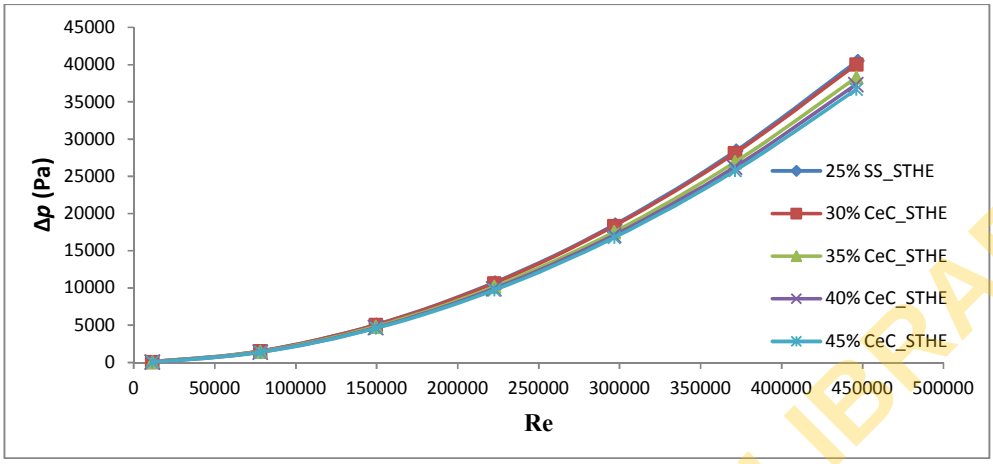

(b) Shell fluid: Water

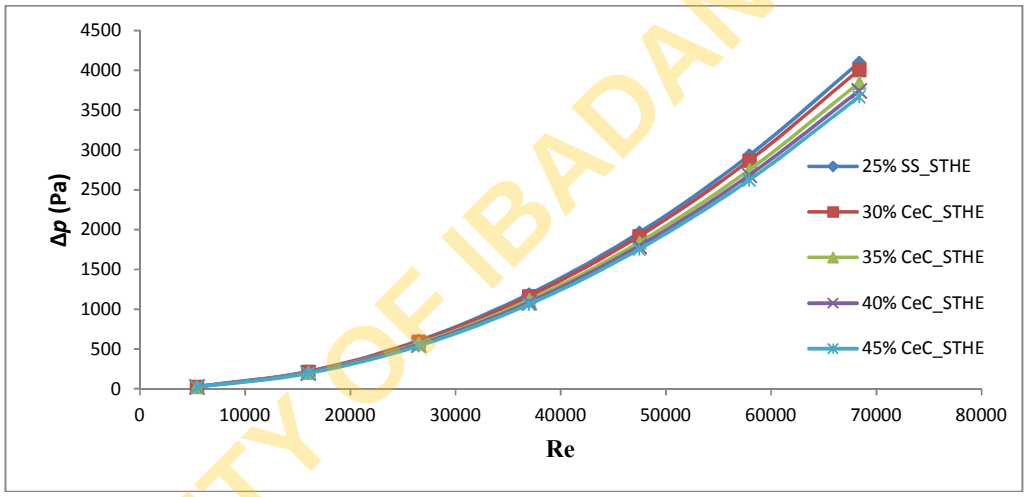

(c) Shell fluid: Air

Fig. 8. The shell-side pressure drop and Reynolds number

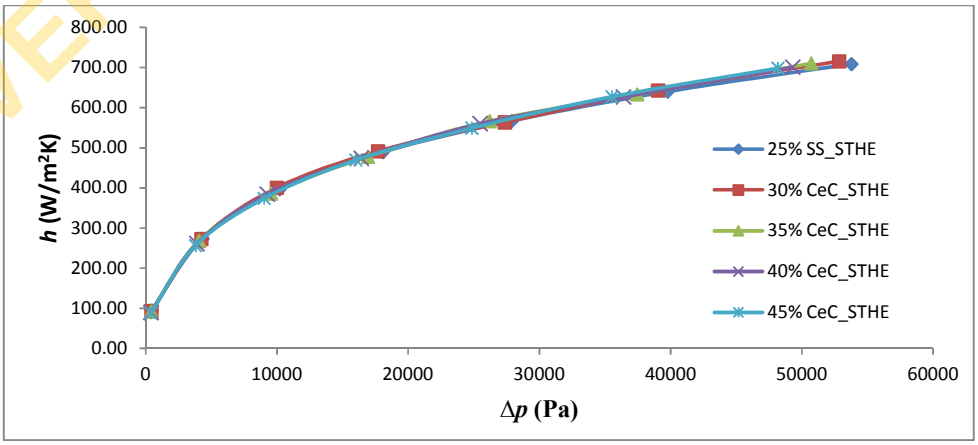

(a) Shell fluid: Engine oil

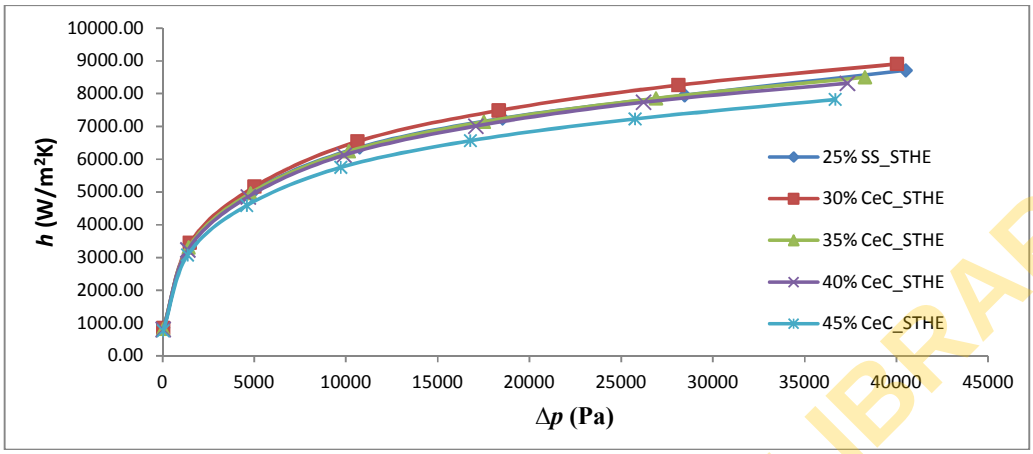

(b) Shell fluid: Water

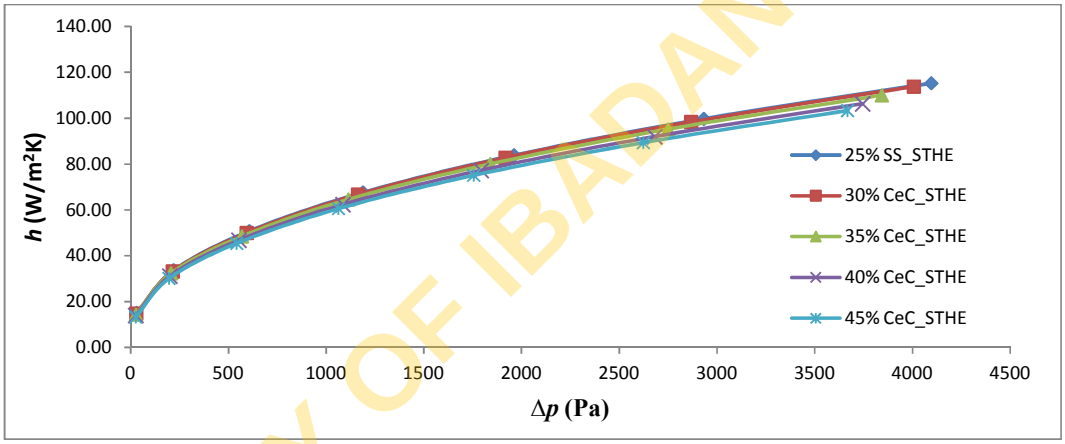

(c) Shell fluid: Air

Fig. 9. Variation of heat transfer coefficient with pressure drop

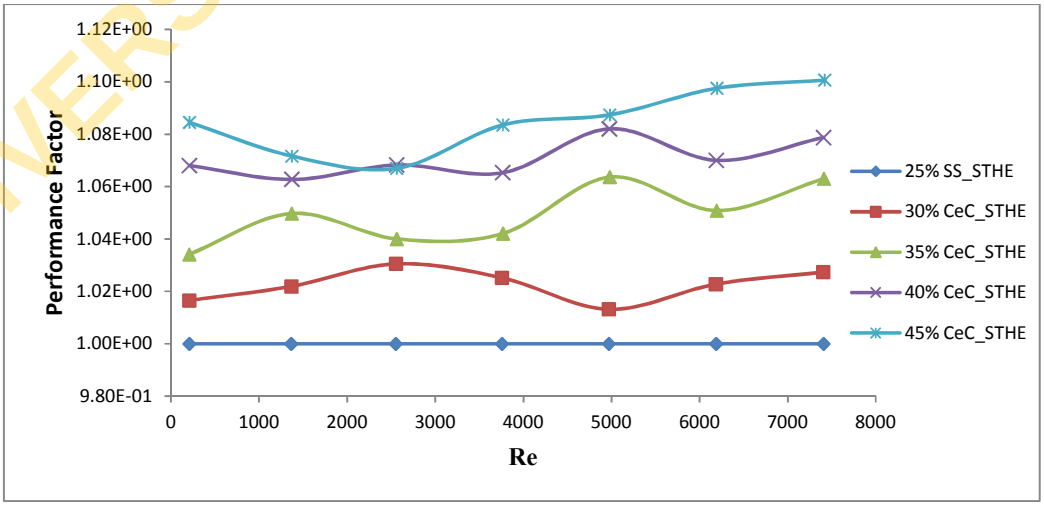

(a) Shell fluid: Engine oil

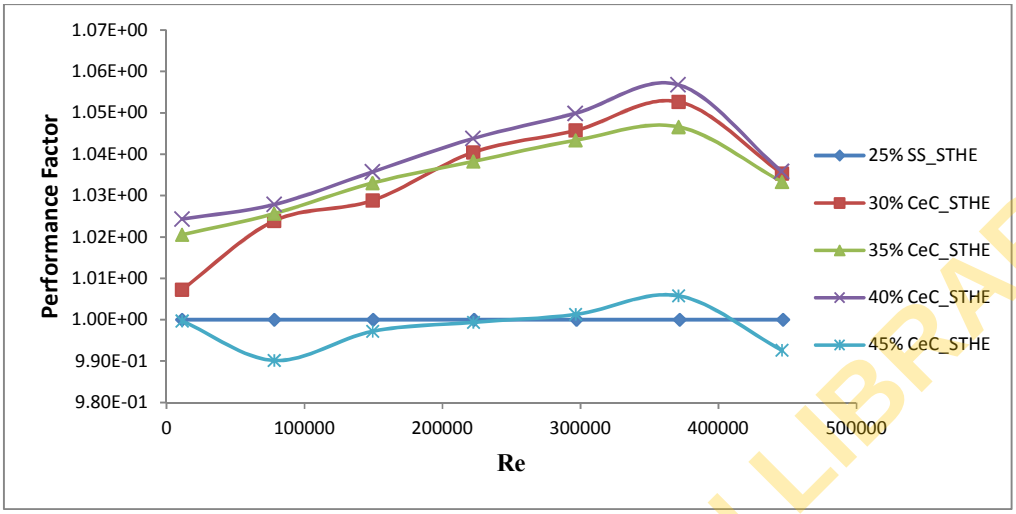

(b) Shell fluid: Water

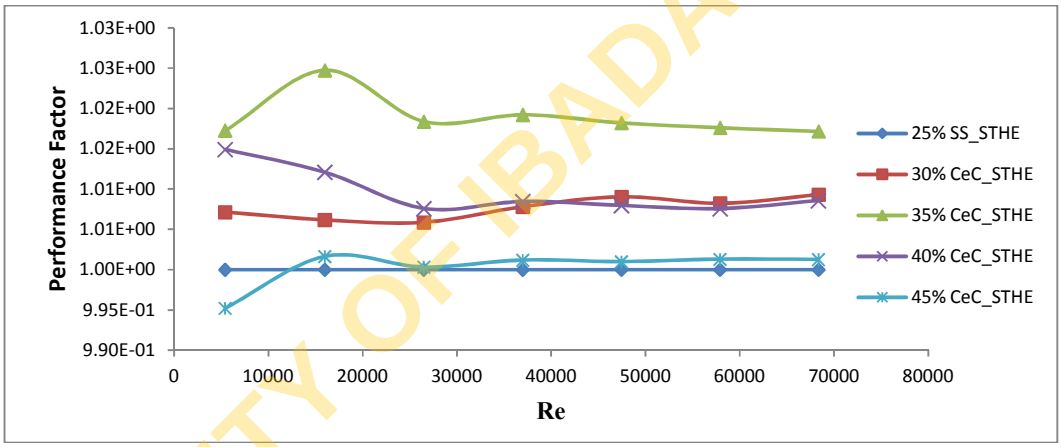

(c) Shell fluid: Air

Fig. 10. The performance factor versus Reynolds number

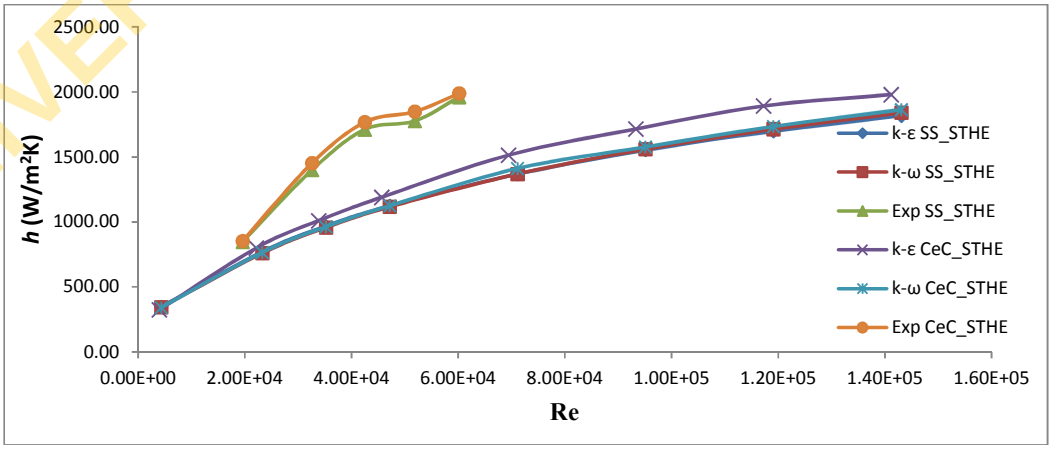

Fig. 11. The performance factor as against Reynolds

Also for SS_STHE, there are positive coefficients of correlation of 0.984 and 0.982 between the experimental results and each of the *k-ε* and *k-ω* numerical results, respectively. Correspondingly for CeC_STHE, they are 0.969 and 0.969.

The variation of the shell-side pressure drop against the Reynolds number obtained from experiment and similar numerical solution are as presented in Fig. 12. The pressure drop still had a steep rise as against the increase in Reynolds number while the SS_STHE demonstrated higher pressure drop in each of the analyses. The comparative differences in results between the SS_STHE and 30% CeC_STHE are 1.09, 1.44 and 2.86% for the experimental, *k-ε* and *k-ω*, respectively. There are positive correlation coefficients between all the results from the experimental and numerical analyses. The coefficients from SS_STHE are 0.996 and 0.996 for *k-ε* and *k-ω*, respectively. In the same order for CeC_STHE, they are 0.994 and 0.993.

3.2.1 Performance from experimental study

The variation of the shell-side heat transfers coefficients versus the pressure drop for the heat exchangers are as shown in Fig. 13. Based on the same range of pressure drop, the weighted shell-side heat transfer coefficient (*WSHTC*) of the 30% CeC_STHE as compared with SS_STHE is 0.028, which implies better performance of 30% CeC_STHE.

Fig. 14 shows the performance factor over a range of Reynolds numbers of the two heat exchangers. The obtained weighted performance factor (*WPF*) for 30% CeC_STHE is 0.038, which also implies better performance.

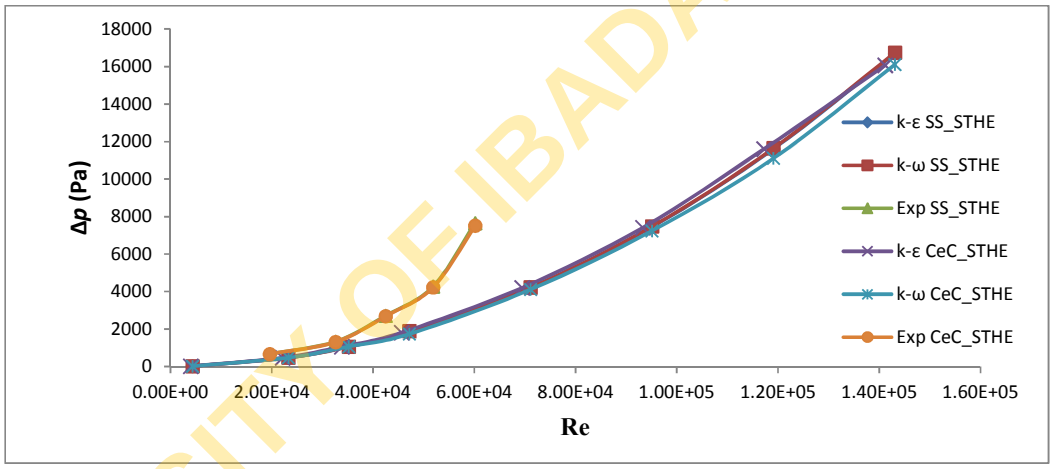

Fig. 12. Pressure drop versus the Reynolds number

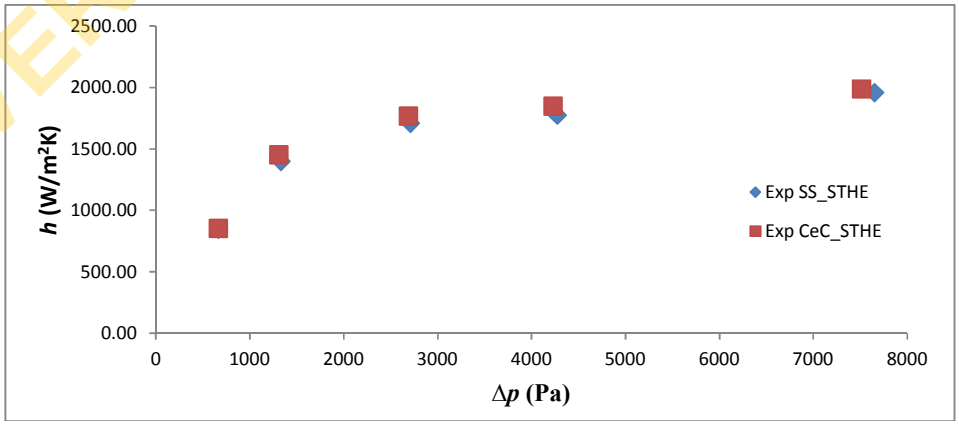

Fig. 13. Heat transfer coefficient versus pressure drop

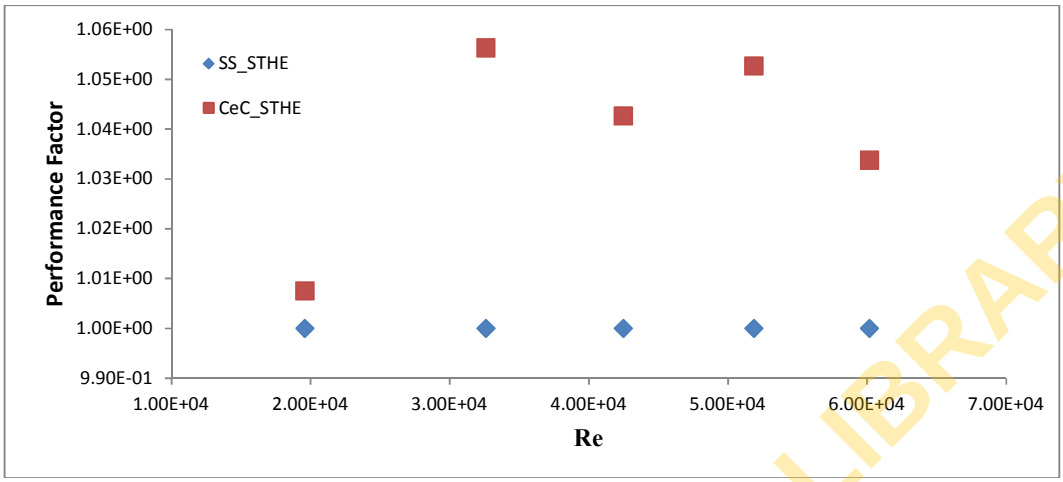

Fig. 14. Performance factor versus Reynolds number

4. CONCLUSION

This study employed numerical and experimental approaches to comparatively investigate the performance of shell-and-tube heat exchanger with single-segmental (SS_STHE) and convex-cut (30, 35, 40 and 45% CeC_STHE) baffles. The numerical analysis was consecutively conducted using water, engine oil and air as shell-side fluids while the experimental analysis was run only on water. It was clearly indicated from the study that the baffle configurations had much influence on the thermal-hydraulic performance of shell-and-tube heat exchanger. Aside the 30% CeC_STHE, all the CeC_STHEs had lower heat transfer coefficients than the SS_STHE. Nevertheless, the SS_STHE exhibited greater pressure drop than the CeC_STHEs. The overall performance of the CeC_STHEs is very fair for all the selected working fluids, CeC_STHEs showed better performance using the weighted performance factor as indicator but perform poorly, with the exception of 30% CeC_STHE, using the weighted shell-side heat transfer coefficient. In all the cases considered cases and for all the working fluids, the 30% CeC_STHE proved to be more suitable in shell-and-tube heat exchanger.

COMPETING INTERESTS

Authors have declared that no competing interests exist.

REFERENCES

1. Wang Y, Gu X, Jin Z, Wang K. Characteristics of heat transfer for tube banks in crossflow and its relation with that in shell-and-tube heat exchangers. Int. J. Heat Mass Transf. 2016;93:584–594.
2. Kallannavar S, Mashyal S, Rajangale M. Effect of tube layout on the performance of shell and tube heat exchangers. Mater. Today Proc; 2019.
3. Labbadlia O, Laribi B, Chetti B, Hendrick P. Numerical study of the influence of tube arrangement on the flow distribution in the header of shell and tube heat exchangers Appl. Therm. Eng. 2017;126:315–321.
4. Bhutta MMA, Hayat N, Bashir MH, Khan AR, Ahmad KN, Khan S. CFD applications in various heat exchangers design: A review. Applied Thermal Engineering. Elsevier Ltd. 2012;32:1–12.
5. Nwokedi IC, Igwegbe CA. Design of shell and tube heat exchanger with double passes. J. Eng. Res. Reports. 2018;3(4): 1–12.
6. Salahuddin U, Bilal M, Ejaz H. A review of the advancements made in helical baffl es used in shell and tube heat exchangers. Int. Commun. Heat Mass Transf. 2015;67:104–108.
7. Wang Q, Chen G, Chen Q, Zeng M. Review of improvements on shell-and-tube heat exchangers with helical baffles. Heat Transf. Eng. 2010;31(10):836–853.
8. Lei Y, Li Y, Jing S, Song C, Lyu Y, Wang F. Design and performance analysis of the novel shell-and-tube heat exchangers with louver baffles. Appl. Therm. Eng. 2017;125:870–879.
9. Petinrin MO, Dare AA. Numerical modelling of effect of baffle orientation offset on shell-and-tube heat exchanger

performance. Int. J. Sci. Eng. Res. 2018;9(2):2096–2108.
10. Nasiruddin, Siddiqui MHK. Heat transfer augmentation in a heat exchanger tube using a baffle. Int. J. Heat Fluid Flow. 2007;28:318–328.
11. Zhang J, He Y, Tao W. A design and rating method for shell-and-tube heat exchangers with helical baffles. J. Heat Transfer. 2010;132:1–8.
12. Mellal M, Benzeguir R, Sahel D, Ameur H. Hydro-thermal shell-side performance evaluation of a shell and tube heat exchanger under different baffle arrangement and orientation. Int. J. Therm. Sci. 2017;121:138–149.
13. El Maakoul A, Laknizi A, Saadeddine S, El Metoui M, Zaite A, Meziane M, Abdellah AB. Numerical comparison of shell-side performance for shell and tube exchangers with trefoil-hole, helical and segmental baffles. Appl. Therm. Eng. 2016;109:175–185.
14. Li H, Kottke V. Analysis of local shellside heat and mass transfer in the shell-and-tube heat exchanger with disc-and-doughnut baffles. Int. J. Heat Mass Transf. 1999;42:3509–3521.
15. Arani AAA, Moradi R. Shell and tube heat exchanger optimization using new baffle and tube configuration. Appl. Therm. Eng. 2019;157:1–11.
16. Liu JJ, Liu ZC, Liu W. 3D numerical study on shell side heat transfer and flow characteristics of rod-baffle heat exchangers with spirally corrugated tubes. Int. J. Therm. Sci. 2015;89:34–42.
17. Naqvi SMA, Elfeky KE, Cao Y, Wang Q. The analysis numerical on performances of shell side segmental baffles, helical baffles and novel clamping anti-vibration baffles with square twisted tubes shell and tube heat exchangers. Energy Procedia. 2019;158(29):5770–5775.
18. Bouhairie S. Selecting baffles for shell-and-tube heat exchangers. Heat Transf. 2012;27–33.
19. Wang Y, Liu Z, Huang S. Experimental investigation of shell-and-tube heat exchanger with a new type of baffles. Heat Mass Transf. 2011;47:833–839.
20. Yang J, Ma L, Bock J, Jacobi AM, Liu W. A comparison of four numerical modeling approaches for enhanced shell-and-tube heat exchangers with experimental validation. Appl. Therm. Eng. 2014;65(1–2): 369–383.
21. Yang J, Liu W. Numerical investigation on a novel shell-and-tube heat exchanger with plate baffles and experimental validation. Energy Convers. Manag. 2015;101:689–696.
22. You Y, Fan A, Lai X, Huang S, Liu W. Experimental and numerical investigations of shell-side thermo-hydraulic performances for shell-and-tube heat exchanger with trefoil-hole baffles. Appl. Therm. Eng. 2013;50:950–956.
23. Yongqing W, Xin G, Ke W, Qiwu D. Numerical investigation of shell-side characteristics of H-shape baffle heat exchanger. Procedia Eng. 2011;18:53–58.
24. Veera Krishna M, Chamkha AJ. Hall and ion slip effects on MHD rotating boundary layer flow of nanofluid past an infinite vertical plate embedded in a porous medium. Results in Physics. 2019;15: 102652.
DOI:https://doi.org/10.1016/j.rinp.2019.102652
25. Veera Krishna M, Swarnalathamma BV, Chamkha AJ. Investigations of Soret, Joule and Hall effects on MHD rotating mixed convective flow past an infinite vertical porous plate. Journal of Ocean Engineering and Science. 2019;4(3):263-275.
DOI:https://doi.org/10.1016/j.joes.2019.05.002
26. Veera Krishna M, Chamkha AJ. Hall effects on MHD Squeezing flow of a water based nano fluid between two parallel disks. Journal of Porous Media. 2019;22(2):209-223.
DOI:https://doi.org/10.1615/JPorMedia.2018028721
27. Mohammadi K, Heidemann W, Müller-Steinhagen H. Numerical investigation of the effect of baffle orientation on heat transfer and pressure drop in a shell and tube heat exchanger with leakage flows. Heat Transf. Eng. 2009;30(14):1123–1135.
28. Leoni GB, Klein TS, Medronho RDA. Assessment with computational fluid dynamics of the effects of baffle clearances on the shell side flow in a shell and tube heat exchanger. Appl. Therm. Eng. 2017;112:497–506.
29. Rahim A, Jameel SMS. Shell side cfd analysis of a small shell-and-tube heat exchanger considering the effects of baffle inclination on fluid flow. In Proceedings of the National Conference on Trends and

Advances in Mechanical Engineering. 2012;167–173.
30. Raj RT, Ganne S. Shell side numerical analysis of a shell and tube heat exchanger considering the effects of baffle inclination angle on fluid flow. Therm. Sci. 2012;16(4):1165–1174.
31. Ozden E, Tari I. Shell side CFD analysis of a small shell-and-tube heat exchanger. Energy Convers. Manag. 2010;51:1004–1014.
32. Tannehill JC, Anderson DA, Pletcher RH. Computational fluid mechanics and heat transfer, 2nd Ed. Washington: Taylor and Francis; 1997.
33. Wilcox DC. Turbulence modeling for CFD, 3rd Ed. California: DCW Industries; 2006.
34. Woelke M. Eddy viscosity turbulence models employed by computational fluid dynamic. Trans. Inst. Aviat. 2007;4(191): 92–113.
35. Böckh P, Wetzel T. Heat transfer: Basics and practice. Berlin Heidelberg: Springer-Verlag; 2012.
36. Gnielinski V, Heat transfer in pipe flow. In: P. Stephan, Editor. In VDI Heat Atlas, 2nd Ed. Berlin Heidelberg: Springer-Verlag. 2010;716–731.
37. Gaddis ES, Gnielinski V. Shell-side heat transfer in baffled shell-and-tube heat exchangers. In: P. Stephan, Editor. In VDI Heat Atlas, 2nd Ed. Berlin Heidelberg: Springer-Verlag. 2010;762–772.
38. Gaddis ES. Pressure drop of tube bundles in cross flow. In: P. Stephan, Editor. In VDI Heat Atlas, 2nd Ed. Berlin Heidelberg: Springer-Verlag. 2010;1099–1114.
39. Wang Q, Chen Q. Chen G, Zeng M. Numerical investigation on combined multiple shell-pass shell-and-tube heat exchanger with continuous helical baffles. Int. J. Heat Mass Transf. 2009;52:1214–1222.
40. Wang Q, Chen G, Zeng M, Chen Q, Peng B, Zhang D, Luo L. Shell-side heat transfer enhancement for shell-and-tube heat exchangers by helical baffles. Chem. Eng. Trans. 2010;21:217–222.
41. Moffat RJ. Describing the uncertainties in experimental results. Exp. Therm. Fluid Sci. 1988;1:3–17.
42. Olivier JA. Single-phase heat transfer and pressure drop of water cooled at a constant wall temperature inside horizontal circular smooth and enhanced tubes with different inlet configurations in the transitional flow regime. Ph.D. Thesis, Department of Mechanical and Aeronautical Engineering, University of Pretoria, Pretoria; 2009.
43. Cengel YA, Cimbala JM. Fluid mechanics: fundamentals and applications, 1st Ed. New York: McGraw-Hill; 2006.
44. Mukherjee R. Effectively design shell-and-tube heat exchangers. Chem. Eng. Prog.; 1998.
45. Zhang M, Meng F, Geng Z. CFD simulation on shell-and-tube heat exchangers with small-angle helical baffles. Front. Chem. Sci. Eng. 2015;9(2): 183–193.

Peer-review history:
The peer review history for this paper can be accessed here:
http://www.sdiarticle4.com/review-history/56417